Physical–Chemical Hybrid Transiency: A Fully Transient Li-Ion Battery Based on Insoluble Active Materials

Yuanfen Chen,[1] Reihaneh Jamshidi,[1] Kathryn White,[1] Simge Çınar,[1] Emma Gallegos,[1] Nastaran Hashemi,[1] Reza Montazami[1,2]

[1]Department of Mechanical Engineering, Iowa State University, Ames, Iowa 50011
[2]Ames National Laboratory, Department of Energy, Ames, Iowa 50011, USA
Correspondence to: R. Montazami (E-mail: reza@iastate.edu)

Received 25 February 2016; accepted 23 May 2016; published online 22 June 2016
DOI: 10.1002/polb.24113

ABSTRACT: Transient Li-ion batteries based on polymeric constituents are presented, exhibiting a twofold increase in the potential and approximately three orders of magnitude faster transiency rate compared to other transient systems reported in the literature. The battery takes advantage of a close variation of the active materials used in conventional Li-ion batteries and can achieve and maintain a potential of >2.5 V. All materials are deposited form polymer-based emulsions and the transiency is achieved through a hybrid approach of redispersion of insoluble, and dissolution of soluble components in approximately 30 min. The presented proof of concept has paramount potentials in military and hardware security applications. © 2016 Wiley Periodicals, Inc. J. Polym. Sci., Part B: Polym. Phys. **2016**, *54*, 2021–2027

KEYWORDS: colloids; degradation; hybrid transiency; Li-ion battery; physical–chemical transiency; swelling; transient batteries; transient electronics

INTRODUCTION Unlike conventional electronics that are designed to last for extensive periods of time, a key and unique attribute of transient electronics is to operate over a typically short and well-defined period, and undergo fast and, ideally, complete self-deconstruction and vanish when transiency is triggered. Transient electronics have a wide range of potential applications including those in healthcare, biomedical devices, environmental sensing/monitoring, green electronics, military and homeland security, to name a few examples. In the very recent years, researchers have developed a wide range of transient electronic devices capable of performing a variety of functions and responsive to a variety of triggering mechanisms including exposure to light,[1] heat[2] or solvent (often aqueous).[3–7] What is common among all these reported transient devices is the need for an external power source. The power is either supplied by inducting coils from a very close distance,[8] or from external power supplies.[2] To realize autonomous transient electronic devices, similar to conventional ones, a transient battery is essential. Thus far, there has been limited efforts in design and construction of transient batteries, mainly due to the lack of soluble proper materials. Jimbo et al. reported swallowable batteries based on Zn and Pt electrodes and ceramic porous separator; maximum potential of 0.42 V and current of 2.41 mA were achieved.[9] More recently, Kim et al. reported edible water activated sodium batteries based on melanin electrodes where a potential of 0.6–1.06 V and current of 5–20 μA, depending on design, was achieved.[10,11] An intrinsically transient battery capable of environmental resorption was first reported by Yin et al. where Mg anode and biodegradable metals (Fe, W, or Mo) cathodes were used with a transient polymer casing; potentials ranging from 0.45 to 0.75 V (depending on cathode materials) were reported.[12] To date, all reported transient batteries have shortcomings compare to their conventional counterparts; uncompetitive potential, current, stability and shelf life are among the top challenges in construction of a practical transient battery that can supply enough power to run a common electric circuit. The low potential and power density in transient batteries are mainly due to the use of non-optimal electrode materials because of their solubility. One other significantly important limitations of transient batteries reported to date is low transiency rate, which is a result of slow chemical reactions between the constituent materials and the solvent. High transiency rates are specially anticipated in military and hardware security applications.

To design a transient battery capable of supplying enough power and undergoing fast transiency, new approaches toward the materials and structural design are necessary.

Lithium-ion battery technology is a well-established, mature, and commercialized technology; here, we are integrating a variation of this technology with our new approach toward

Additional Supporting Information may be found in the online version of this article.

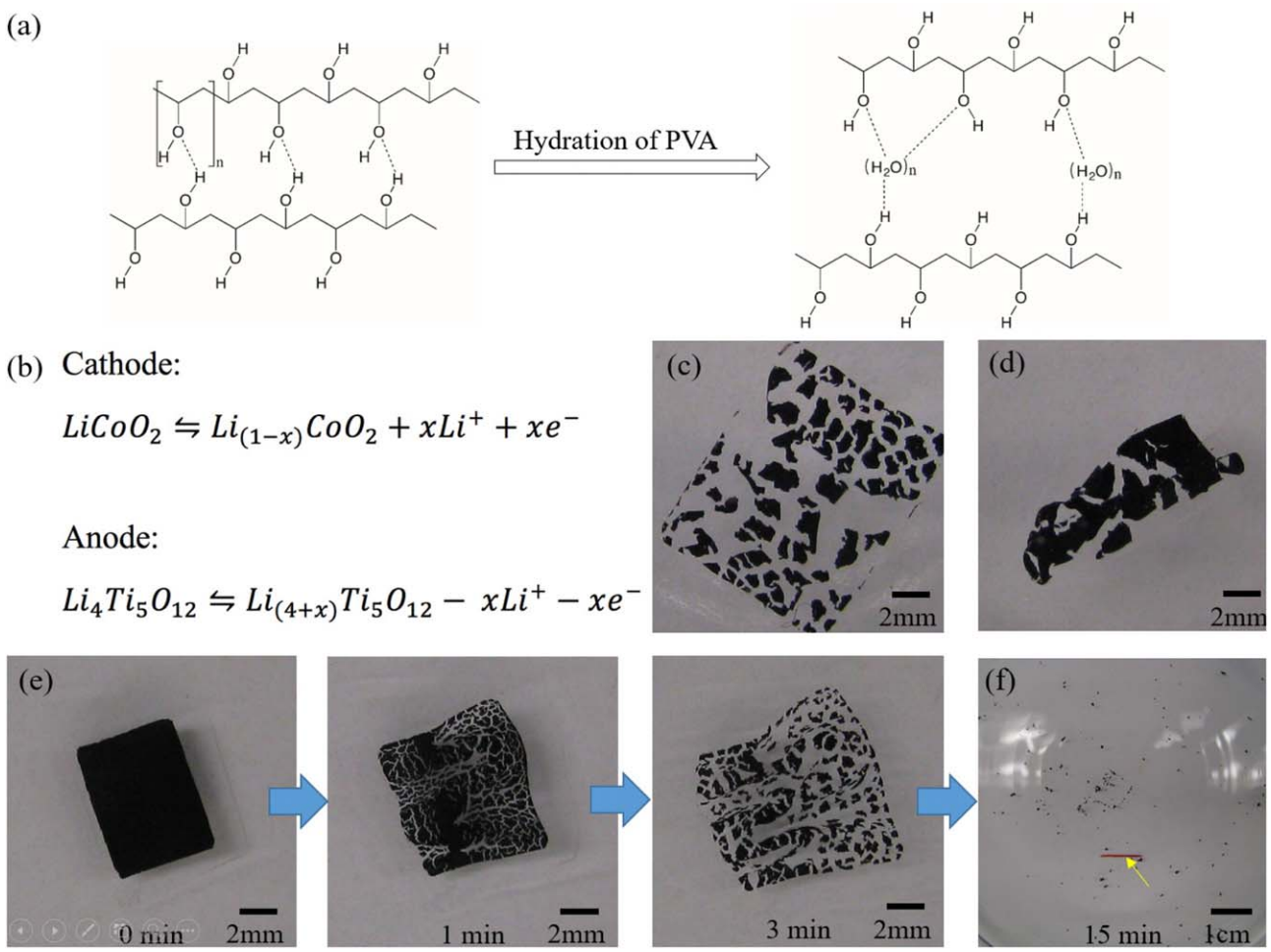

FIGURE 1 (a) Hydration of PVA which results in swelling of the polymer membrane, PVA repeat unit is identified on the top left of the figure; (b) half reactions take place at the electrodes; (c) swelling and (d) curling of electrodes with high area density layers of active materials after 3 min of exposure to water; despite fragmentation of the active materials, deconstruction and transiency did not occur; (e) sequential images of transience of a cathode electrode with low area density layer of active materials, the swelling force is large enough to deconstruct the electrode; (f) dissolution of soluble and redispersion of insoluble constituent materials leads to full transiency, the yellow arrow points at a scale bar drawn in the background. Note that scale bar on (f) is different. [Color figure can be viewed in the online issue, which is available at wileyonlinelibrary.com.]

transient electronics, which is ultimately based on a hybrid approach of physical redispersion of insoluble materials, and chemical dissolution of soluble ones. In our previous studies, we have reported electrical[13] and mechanical[14] properties of such hybrid systems. The transient primary Li-ion batteries we report here incorporate this technology and are consist of electrodes comprise of active materials similar to those in conventional Li-ion batteries while swelling force of the substrate/casing materials is utilized to introduce transiency through fragmentation and redispersion of the active materials.

Due to its ease of control over transiency rate and fabrication, PVA and PVA composites were used as binder, substrate, and casing materials. Abundance of hydroxyl groups in PVA allows high equilibrium swelling indices, up to 153% in water.[15] Hydration of PVA results in disentanglement of polymer chains and leads to swelling of the polymer membrane [Fig. 1(a)]. In PVA-sucrose composites, presence of fast-dissolving sucrose expedites the process by opening up voids in the structure that enhance penetration of water. Subsequently, PVA chains are eventually solvated and the membrane dissolves in the solvent. Lithium cobalt oxide, $LiCoO_2$, (LCO), and $Li_4Ti_5O_{12}$ (LTO) were used as the ultimate cathode and anode active materials, respectively. Cathode and anode half reactions[16] are shown in Figure 1(b). PVA and carbon black were used as binder and filler in LCO and LTO to form water-deconstructible nanostructures. Presence of PVA and carbon black in LCO and LTO increases uniformity of the electrodes while also enhancing redispersion of the materials when triggered; on the other hand, efficiency of the electrodes drops due to the lack of electron conductivity in PVA. Active materials (LCO/LTO-PVA-carbon black aqueous emulsion) were deposited via spray coating over a stencil mask. Systematic studies of electrode components revealed that the thickness of active materials coating

TABLE 1 Transiency Test on Samples with Varying Area Density of the Active Materials

Area density of active materials (mg cm^{-2})	1.2 ± 0.1	1.6 ± 0.1	2.3 ± 0.2
Fragment average area (mm^2)	~0.77	~1.82	~4.4
Electrode-substrate delamination	Yes	No	No
Outcome	Transiency	Sample curled	Sample curled

is the defining factor on whether or not the electrode fully disintegrates, where no dependence on the thickness of the PVA-sucrose substrate was observed. Cathode electrodes with active materials area densities ranging from 1 to 2.5 mg cm^{-2} [categorized in three groups: (1) 1.2 ± 0.1, (2) 1.6 ± 0.1, and (3) 2.3 ± 0.2 mg cm^{-2}] were fabricated on PVA:sucrose (10:1 wt ratio) substrates of thicknesses ranging from 30 to 80 μm (categorized in six groups, 10 μm increments). PVA at this particular composition was selected for its fast and controllable transience rate based on our previous work.[17] Regardless of the thickness of substrate, when exposed to the solvent, electrodes with active materials' area densities of 1.5 mg cm^{-2} or higher only curled and/or swelled but did not disintegrate nor exhibit transiency [Fig. 1(c,d)]. For active materials area densities of 1.3 mg cm^{-2} or lower (Group 1), the electrodes swelled and the swelling force was large enough to fragment and deconstruct the whole electrode, regardless of the thickness of the substrate. Fragment average area (average size of fragments due to crack propagation) was smaller for electrodes with smaller active materials area density, see Table 1 and Figure 1(c–f). As the solvent molecules penetrate through the substrate, swelling force is generated and increased to a point large enough to physically break the active materials layer [Fig. 1(e)].[14] Swelling of PVA and the associated force which breaks the active materials into pieces are essential to the transiency of the electrode; an identical sample of active materials (same area density) on polyvinyl acetate substrate (does not swell but dissolve in water) only curled and did not break or exhibit transiency (Supporting Information Fig. S1). After initial swelling, the substrate is eventually dissolved and resorbed into the aqueous environment; subsequently, PVA binder in the remaining pieces of the active materials also dissolves which enhances redispersion and transiency of the active materials in the solvent [Fig. 1(f)]. Summarized in Table 1 are the experimental data collected and outcomes for variety of cathodes structures. Results revealed that electrodes with small area density are essential for construction of a transient battery. Similar study on anodes resulted in comparable conclusions.

Single-cell batteries were constructed by fabrication of current leads and active materials on PVA-based substrates; substrates were featured by grooves to hold current leads. A cellulose-based porous membrane (short fibers thus water decomposable) was used as the separator and electrolyte holder between the electrodes; and, battery was formed and sealed by attaching the uncoated margins of the PVA-based electrodes together. $LiPF_6$-based electrolyte was then injected into the separator and the hole was sealed. Presented in Figure 2(a) is a schematic representation of cross section of a single cell battery. Electrodes were fabricated with characteristics of Group 1 electrodes as presented in Table 1. Carbon black and silver paint were used for fabrication of current leads; while the silver paint has higher electrical conductivity, only carbon black was used as the cathode current lead to prevent oxidation of silver in cathode when under applied potential (charging). The single cell batteries were charged and discharged couple of times before the transiency testing to ensure proper functionality of the battery. Heat generated during this process strengthen the bonding among the materials and slightly hindered transiency rate compare to that of single -unheated- electrodes. Thus, although active materials used in this study are most suitable for secondary cell batteries, we report the constructed batteries as primary cell that require an initial charging and can undergo few charging/discharging cycles in practice. Yet, it must be noted that cycling the cell will result in chemical reactions among constituent elements that hinder transiency.

To evaluate transiency of the single cell batteries [Fig. 2(b)], DI water at room temperature was used as a trigger (solvent). As expected from single electrode experiments, the single cell swelled and the electrodes cracked moments after exposure to the solvent; yet, it took a longer time for substrate to dissolve and active materials to redisperse. Demonstrated in Figure 2(c) are sequential images of the transience of the battery. The substrate swells first witch results in physical deconstruction of the electrodes. Initially the current leads are less impacted as the thickness of those areas is greater than that of the rest of the electrode. The anode cracked into larger pieces while the cathode deconstructed into much smaller ones [see Fig. 2(c) at 5.5 min]. Eventually the substrate dissolved completely and electrode remains were released to roam freely in the solvent. Dissolution of the PVA binder in the active materials resulted in dispersion of milli/micrometer size particles in the solvent. After approximately 30 min, most of the battery was either dissolved or redispersed. Remains were left for another 16.5 h to redisperse; although the remaining pieces reduced in size over time, the change was incremental between the 1st and 17th h. The overall transience behavior was similar to that of the single electrodes, yet expanded over a longer period of time. The extended time was anticipated to be consequent to 1) increase of the overall thickness of the battery compare to single electrode; and 2) induced bonding due to the heat generated during charging and discharging.[18,19]

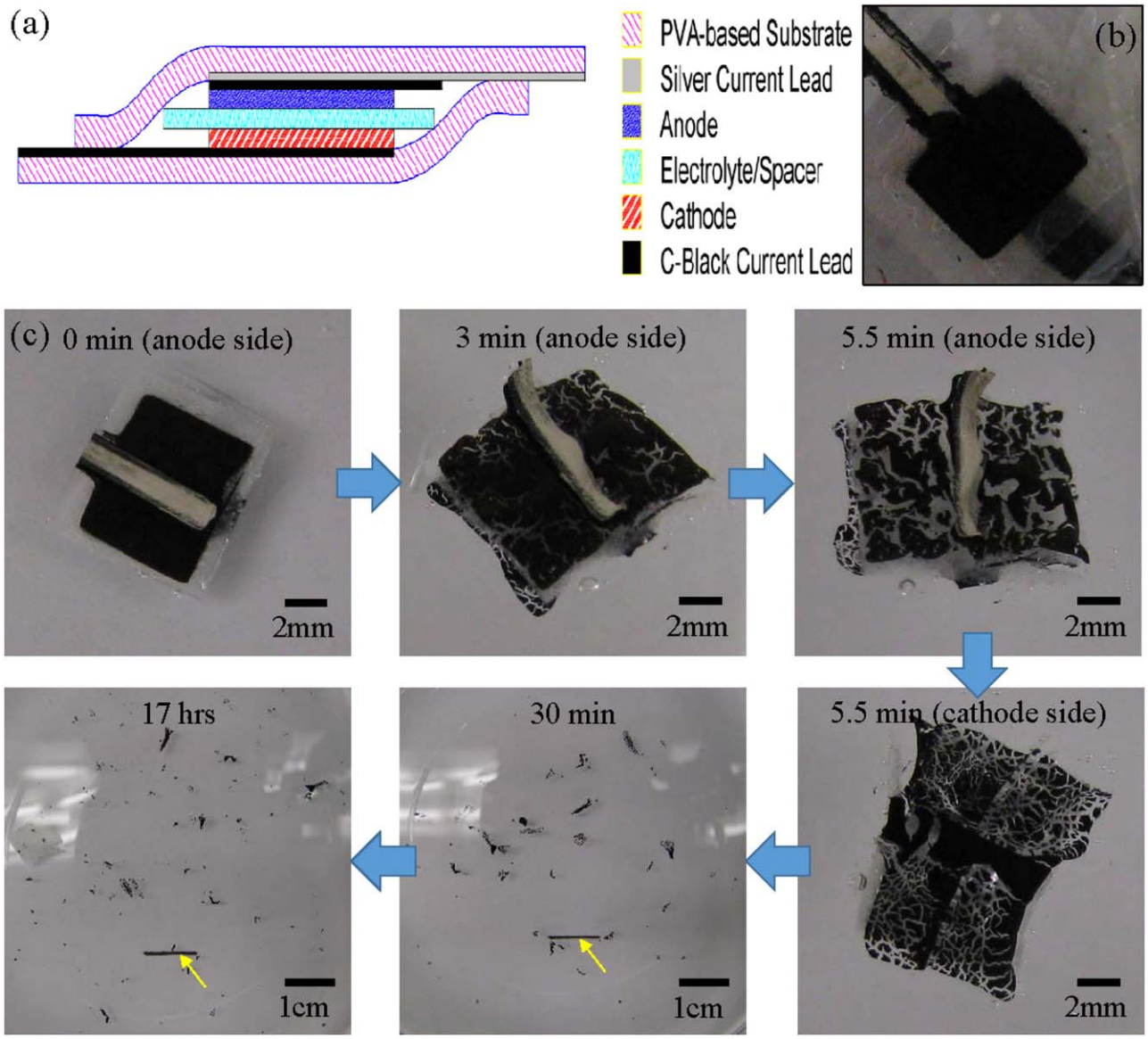

FIGURE 2 (a) Schematic representation of the cross section of the battery cell; (b) a transient battery cell; (c) sequential images of transience of a battery cell, the yellow arrows point at scale bars drawn in the background. Note that scale bars on the last two images are different. [Color figure can be viewed in the online issue, which is available at wileyonlinelibrary.com.]

The performance of the single cell transient batteries were evaluated at different discharge current densities of 10, 20, and 50 μA cm^{-2}; and, cut-off voltages of 2.7 V (charge) and 1.0 V (discharge). As demonstrated in Figure 3(a), the battery has comparable performances at different discharge current densities. The discharge voltages start at approximately 2.6 V, slowly decrease to 1.8 V, and then drop to 1.0 V at sharp slopes. The battery cell had the highest discharging specific capacity (~2.27 mAh g^{-1}) and efficiency (12.5%), and total capacity of 0.571 μAh when discharged at 20 μA cm^{-2}. Typically, the discharging capacity decreases as the discharging current increases; in our study, however, the battery has higher discharging specific capacity at 20 μA cm^{-2} compared to 10 μA cm^{-2} mainly because of the relatively high internal resistance of the battery. At 50 μA cm^{-2} discharging current density the reaction time is deemed to be the limiting factor for higher discharging specific current; thus, the 20 μA cm^{-2} discharging current density exhibited the highest discharging specific capacity for this cell configuration. Shown in Figure 3(b) is the discharging potential as a function of time.

The electrochemical reactions occurring at the electrodes/electrolyte interfaces determine the electrochemical performance of the battery. To evaluate the parameters involved in the electrochemical processes, the electrochemical impedance of the battery was measured over a wide frequency range [Fig. 3(c,d)]; an equivalent circuit was introduced based on Randles cell model[20] to fit the data of electrochemical impedance Nyquist plot. The impedance at low frequency range (between 0.1 and 1.0 Hz) is between 10 and

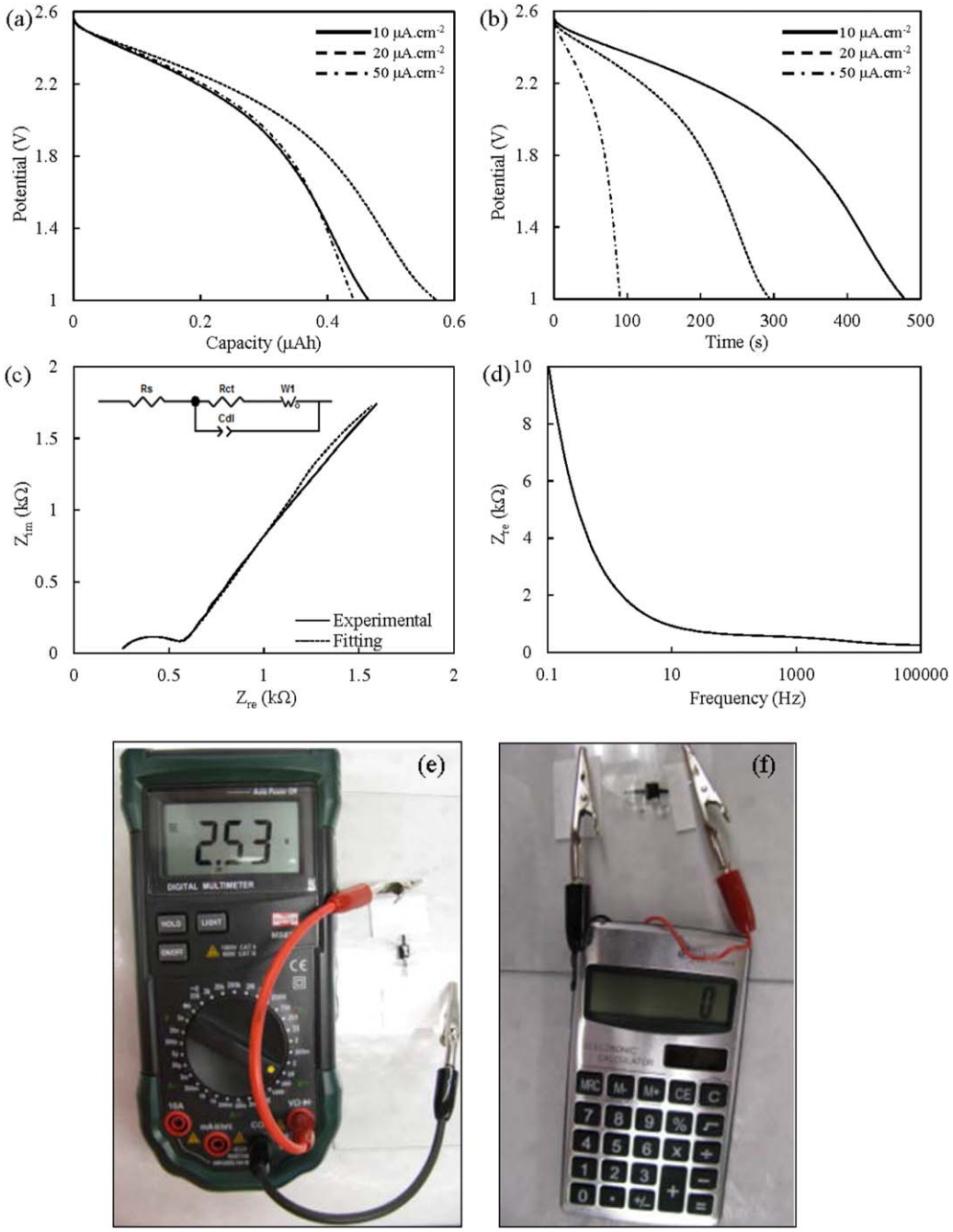

FIGURE 3 (a) and (b) Discharging behavior of transient battery cells at different current densities; (c) and (d) electrochemical impedance of a battery cell and the equivalent electric circuit (c inset); (e) a battery cell connected to a digital multimeter, and (f) transient battery cell utilized to power a calculator (battery and solar panel are disconnected from the calculator's circuit). [Color figure can be viewed in the online issue, which is available at wileyonlinelibrary.com.]

2.5 kΩ [Fig. 3(d)]. The Nyquist plot presented in Figure 3(c) consists of a depressed semicircle at high frequency, which is an indication of non-uniform electrode/electrolyte interfaces, and a linear spike at low frequency. The equivalent circuit [Fig. 3(c), inset] consists of two resistors: R_s corresponding to the ohmic resistance at high frequency and R_{ct} corresponds to the charge transfer resistance of the electrodes, a Warburg element (W) which accounts for the diffusion reactance at low frequencies, and a constant phase element (CPE) corresponding to the double layer charging (C_{dl}) at the porous electrode/electrolyte interfaces; CPE is used instead of an ideal capacitor because of the depressed shape of the Nyquist semicircle.[21] Results suggest an R_s value of approximately 242 Ω, which includes the electrolyte resistance as

well as the ohmic resistance of the battery cell and an R_{ct} of approximately 327 Ω. The relatively large value of R_{ct} is presumed to be an indication of poor connection between the electrodes and electrolyte layer. While both non-uniform interfaces and presumably poor connections between the battery components may be responsible for relatively poor electrochemical performance of the presented battery cell, they are not fundamental issues and could be improved by utilization of advanced manufacturing techniques.

Shown in Figure 3(e) is a battery cell connected to a digital multimeter, showing 2.53 V potential that is double the initial potential (prior to transiency initiation) of transient electrodes reported in the literature.[9–12] A single battery cell is capable to supply enough power to power a basic calculator for a short period of time; the threshold voltage to power the calculator is ∼1 V. Presented in Figure 3(f) is a battery cell powering a four-function calculator. The battery and solar cell of the calculator were disconnected from the device's circuit and the power was only supplied by the transient battery. The battery cell was able to power the calculator for approximately 15 min before the screen started to fade. Fabricating electrodes with higher area density or connecting several battery cells in parallel can significantly improve the performance of the battery for higher power consuming applications; yet, higher area density electrodes take longer time to deconstruct. Also, as discussed earlier, more advanced fabrication techniques can be used to improve the overall efficiency and performance of battery cells, while transiency rate can be controlled via optimization of the nano/microstructure of electrodes and substrate.

EXPERIMENTAL

Materials

Polyvinyl alcohol (PVA) (Mw: 61,000 g mol^{-1}, 98.0–98.8% hydrolyzed), sucrose, lithium hexafluorophosphate ($LiPF_6$), ethylene carbonate (EC) and dimethyl carbonate (DMC) were purchased form Sigma Aldrich (Sigma Aldrich, MO, USA) and used as received. $LiCoO_2$, (LCO) powder, $Li_4Ti_5O_{12}$ (LTO) powder, and carbon black were purchased from MTI (MTI Corporation, CA) and used as received. Commercially available short fiber cellulose based tissue was used as separator. Silver paint was purchased form Ted Pella (Ted Pella, CA) and diluted with acetone (1:1 vol).

Substrate

About 1.0 g PVA, 0.1 g sucrose, and 50 μL of 1 M aqueous HCl solution were added to 20 mL of DI water. The solution was stirred at 70 °C for 4 h, then cooled down to room temperature and stirred for 2 additional h. The clear solution was then casted onto a plastic mold (with14 mm × 1.2 mm × 0.1 mm grooves for current leads) and dried at ambient conditions for 24 h. The dried PVA film was peeled off of the mold carefully and used as the substrate for cathode and anode.

Active Materials

To prepare Cathode active material 1.0 g PVA was dissolved in 20 mL of DI water and stirred at 70 °C for 4 h. 5.15 g LCO powder and 1.0 g carbon black were added to the PVA solution and stirred for 2 h to get uniform emulsion. Anode active material was prepared in the same manner with the exact same ratios and procedure as cathode, where LCO was substitute by LTO.

Current Leads

One gram PVA was dissolved in 20 mL of DI water as described above, carbon black was added at 3:2 wt ratio (3 carbon black) and stirred for 2 h to obtain a uniform emulsion. Silver paint was diluted with acetone (1:1 vol ratio). Current lead at anode was fabricated by spraying 60-μm-thick layer of silver in the groove of PVA substrate; then, an approximately 50-μm-thick layer of carbon black-PVA emulsion was spray coated on top of the silver layer at slightly wider (∼500 μm) area to cover the silver coating. Stencils were used at both steps. Current lead at cathode was fabricated by spraying a 110-μm-thick layer of carbon black-PVA emulsion through a stencil in the groove of PVA substrate.

Electrodes

About ∼25-μm-thick layers of anode and cathode active materials were spray coated through stencils over the current leads on PVA substrates to form the electrodes. The areas covered by active materials were smaller than the substrate area to allow PVA edge for packing.

Packaging

Cathode, anode, and cellulose-based porous membrane were brought together to form a stack. Uncoated edges of PVA substrates were dampened slightly to bond and seal the stack to form a battery cell.

Electrolyte

About 1 M solution of $LiPF_6$ in 1:1 mixture of EC:DMC was used as the electrolyte. Electrolyte (25 μL) was injected into the packed battery cell by a syringe and pierced area was sealed. All steps involving electrolyte were carried out in a glovebox under nitrogen environment.

Electrochemical Testing

The electrochemical testing and impedance measurements were carried out on a VersaSTAT-4 potentiostat (Princeton Applied Research). The battery was charged and discharged at 2.7 and 1.0 V, respectively, and discharge current densities of 10, 20, and 50 $\mu A.cm^{-2}$. The internal resistance of the battery cell was measured at frequencies between 1.0E5 and 0.1 Hz and a potential difference (ΔV) of 10 mV. The Z-view software was used to obtain the equivalent electric circuit and fit experimental data.

ACKNOWLEDGMENTS

This work was supported in part by Iowa State University PIIR (Presidential Initiative for Interdisciplinary Research) grant. R. Montazami thanks Ashley Christopherson for her help and contribution to this research paper by providing scientific illustrations.

REFERENCES AND NOTES

1 H. L. Hernandez, S. K. Kang, O. P. Lee, S. W. Hwang, J. A. Kaitz, B. Inci, C. W. Park, S. Chung, N. R. Sottos, J. S. Moore, J. A. Rogers, S. R. White, *Adv. Mater.* **2014**, *26*, 7637–7642.

2 C. W. Park, S. K. Kang, H. L. Hernandez, J. A. Kaitz, D. S. Wie, J. Shin, O. P. Lee, N. R. Sottos, J. S. Moore, J. A. Rogers, S. R. White, *Adv. Mater.* **2015**, *27*, 3783–3788.

3 S. W. Hwang, H. Tao, D. H. Kim, H. Cheng, J. K. Song, E. Rill, M. A. Brenckle, B. Panilaitis, S. M. Won, Y. S. Kim, Y. M. Song, K. J. Yu, A. Ameen, R. Li, Y. Su, M. Yang, D. L. Kaplan, M. R. Zakin, M. J. Slepian, Y. Huang, F. G. Omenetto, J. A. Rogers, *Science* **2012**, *337*, 1640–1644.

4 S. W. Hwang, D. H. Kim, H. Tao, T. I. Kim, S. Kim, K. J. Yu, B. Panilaitis, J. W. Jeong, J. K. Song, F. G. Omenetto, *Adv. Funct. Mater.* **2013**, *23*, 4087–4093.

5 S. W. Hwang, G. Park, H. Cheng, J. K. Song, S. K. Kang, L. Yin, J. H. Kim, F. G. Omenetto, Y. Huang, K. M. Lee, *Adv. Mater.* **2014**, *26*, 1992–2000.

6 M. Irimia-Vladu, *Chem. Soc. Rev.* **2014**, *43*, 588–610.

7 M. Irimia-Vladu, E. D. Głowacki, G. Voss, S. Bauer, N. S. Sariciftci, *Mater. Today* **2012**, *15*, 340–346.

8 Hwang, S. W. Huang, X. Seo, J. H. Song, J. K. Kim, S. Hage, -Ali, S. Chung, H. J. Tao, H. Omenetto, F. G. Ma, Z. *Adv. Mater.* **2013**, *25*, 3526–3531.

9 H. Jimbo, N. Miki, *Sens Actuators B: Chem.* **2008**, *134*, 219–224.

10 Y. J. Kim, S. E. Chun, J. Whitacre, C. J. Bettinger, *J. Mater. Chem. B* **2013**, *1*, 3781–3788.

11 Y. J. Kim, W. Wu, S. E. Chun, J. F. Whitacre, C. J. Bettinger, *Proc. Natl. Acad. Sci. USA* **2013**, *110*, 20912–20917.

12 L. Yin, H. Cheng, S. Mao, R. Haasch, Y. Liu, X. Xie, S. W. Hwang, H. Jain, S. K. Kang, Y. Su, *Adv. Funct. Mater.* **2014**, *24*, 645–658.

13 R. Jamshidi, S. Çinar, Y. Chen, N. Hashemi, R. Montazami, *J. Polym. Sci. Part B: Polym. Phys.* **2015**, *53*, 1603–1610.

14 S. Çınar, R. Jamshidi, Y. Chen, N. Hashemi, R. Montazami, *J. Polym. Sci. Part B: Polym. Phys.* **2016**, *54*, 517–524.

15 J. Krzeminski, H. Molisak-tolwinska, *J. Macromol. Sci. Part A: Chem.* **1991**, *28*, 413–429.

16 L. Aldon, P. Kubiak, M. Womes, J. Jumas, J. Olivier-Fourcade, J. Tirado, J. Corredor, C. Pérez Vicente, *Chem. Mater.* **2004**, *16*, 5721–5725.

17 H. Acar, S. Çınar, M. Thunga, M. R. Kessler, N. Hashemi, R. Montazami, *Adv. Funct. Mater.* **2014**, *24*, 4135–4143.

18 N. Sato, *J. Power Sources* **2001**, *99*, 70–77.

19 S. A. Khateeb, S. Amiruddin, M. Farid, J. R. Selman, S. Al-Hallaj, *J. Power Sources* **2005**, *142*, 345–353.

20 J. E. B. Randles, *Discuss. Faraday Soc.* **1947**, *1*, 11–19.

21 S. Rodrigues, N. Munichandraiah, A. Shukla, *J. Solid State Electrochem.* **1999**, *3*, 397–405.